Full Length Article

Analysis, design and experimentation of Switched Reluctance Hub Motor

Lenin Natesan Chokkalingam [a], Sanjeevikumar Padmanaban [b,*], Pierluigi Siano [c], Ahmet H. Ertas [d], Chandrasekar Viswam [e], Arumugam Rengaswamy [f]

[a] School of Electrical and Electronics Engineering, Vellore Institute of Technology University, Chennai 600 127, India
[b] Ohm Technologies, Research and Development, Chennai, Tamil Nadu 600122, India
[c] Department of Industrial Engineering, University of Salerno, Campus of Fisciano, Salerno, Italy
[d] Biomedical Engineering Department, Engineering Faculty, Karabuk University, Demir-Celik Campus, Balıklarkayası Mevkii, 78050 Karabuk, Turkey
[e] Kingston College of Engineering, Vellore 632059, India
[f] SSN College of Engineering, Chennai 603110, India

A B S T R A C T

Switched Reluctance Hub Motors (SRHMs) are well suited for electric vehicle (EV) applications due to their numerous advantages, such as simple and rugged construction, low weight, potentially low production cost, easy cooling, excellent torque-speed characteristics, high torque density, high operating efficiency, highly reliable and simple drive train system. This paper provides a complete design and analysis of a three phase 6/8 pole SRHM. The electromagnetic, vibration and acoustic noise possessions are predicted using analytical concepts and finite element analysis (FEA) tools. Finally test results are compared with the FEA results.

© 2016 The Authors. Production and hosting by Elsevier B.V. on behalf of Karabuk University. This is an open access article under the CC BY-NC-ND license (http://creativecommons.org/licenses/by-nc-nd/4.0/).

1. Introduction

In the automotive industry, there is a fast growing interest in the electric drive technology. With great concern for clean environment, different types of motor drive systems such as the permanent magnet motors and switched reluctance motors (SRMs) are being experimented on the automobiles. In this research, hub motors operating on the principle of torque production due to reluctance variation is taken up for the investigation. Within every wheel, there can be one "Direct Drive In-Wheel Motor" to generate the necessary torque per wheel. Unlike conventional "central drive unit" systems, torque, power and speed can be supplied to each tire independently. A 4-phase in-hub miniature SRM with the outer rotor structure for the spindle motor in hard disc drive was discussed in [1]. Sizing the SRM for EVs was developed in [2]. Design procedure for an in-wheel motor had been outlined in [3]. Luk et al. [4] experimented an In-Wheel motor drive with a yokeless rotor. A hybrid switched reluctance motor drive, which is suitable for EVs, was developed in [5]. Comparative design and analysis of 3 phase SR machine topologies for EV propulsion had been found in [6]. A

multi objective design optimization of an in-wheel motor was developed and tested in [7]. Recently, fault tolerant In-Wheel motor for high performance EVs and design consideration for radial flux permanent magnet hub motor has been discussed in [8,9].

A 4 phase SRM has been designed and fabricated for an electric drive-train for campus two wheeler. Field weakening capability of the electric motor should be used to achieve better efficiency. Such a motor tends to have large size due to high base torque rating. Hence, a planetary gear was used to reduce motor's torque rating [12]. Outer-rotor type multi polar Switched Reluctance Hub Motor was implemented for electric drive system. The developed motor has been controlled by asymmetric bridge converter. The high speed-coupler sensor used here provides an accurate measurement of actual rotor position necessary for proper commutation of the designed converter circuit [13]. A three-phase, external-rotor SRM 'with 10 rotor poles and 6 stator poles has been developed for a 500-W electric bike. With a reduction gearbox, the electric bike speed can be restrained under 32 km/h [14]. This paper provides a complete guide to design a SRM hub motor for electric vehicle application.

The paper is organized into five sections. Section 2 gives the constructional details, analytical design and FEA results of SRHM. Section 3 describes the fabrication and testing of the designed SRHM. Section 4 investigates and tested the presence of vibration

and acoustic noise in the fabricated SRHM. Section 5 concluded the study carried out in this paper.

2. Design and analysis of SRHM

The SRHM is a singly excited motor with salient poles on both stator and the rotor. Fig. 1 explains the constructional features of SRHM. The main difference between SRM and SHRM is, the inner member in SRHM is stationary and holds windings; the outer member is rotating, the reversal is the case in SRM.

2.1. Design of SRHM

Process of designing SRHM starts with the design requirements. The design should make sure that all the design requirements are met. Recently available motors in the market for Electric bi-cycle use gears. Motors are rated 262 W with a maximum torque of 15 N m. Gear ratio of 6 is common in many of the motors. The present design aims at designing a SRHM with a gear with ratio of 6. So, the rated torque of the machine is 2.5 N m. The dimensions and design requirements are enumerated in Table 1. The analytical design process has been done using [10]. The dimensions of various parts of the machines are tabulated in Table 2.

2.2. Design verification

2-D FEA is used to verify the design procedure of the SRHM. Using a commercial finite element analysis software package, the flux linkages and the inductances of the phase windings, the torque developed by the SRHM for various rotor positions are determined.

2.3. Finite element analysis

In finite element analysis, the original field problem domain is divided into a number of sub domains of elements. Fig. 2 shows the 2-D FEA model of SRHM, for which dimensions have been obtained. The entire problem region is subdivided into 29865 nodes triangular finite elements.

Figs. 3 and 4 show flux density distribution on steel parts of the machine. In the unaligned position, flux density in the stator lamination is 0.26 T and in an intermediate position, the maximum flux density is 0.8 T.
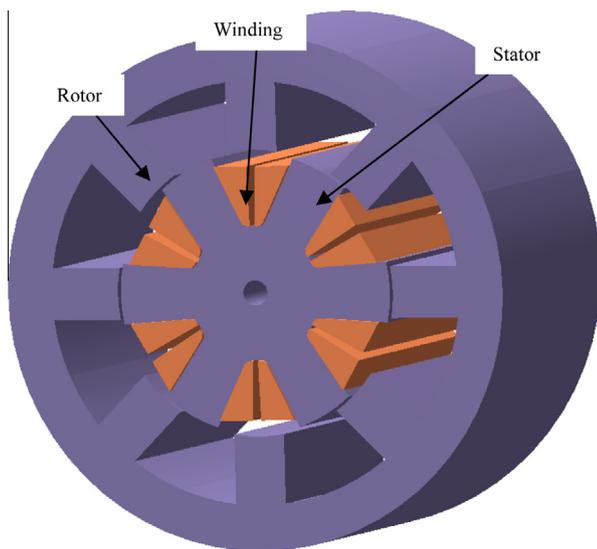
Table 1
Design requirements of SRHM.

Parameters	Specification
Mechanical power output	262 Watts
Normal speed	1000 rpm
Torque-before gear	15 N m
Torque-after gear	2.5 N m
Gear ratio	6
Battery supply voltage	36 V
Phase current	7 A
Rotor outer diameter	130 mm
Machine axial length	50 mm

Table 2
Dimensions of SRHM.

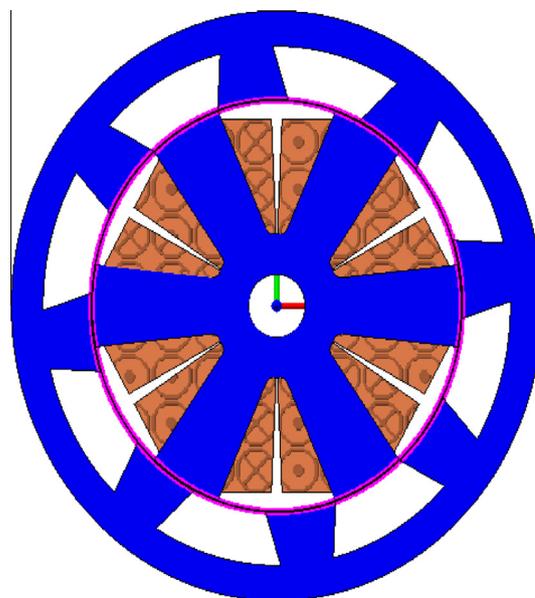| Parameters	Specification
Supply voltage	36 V
Rated current	7 A
Rated speed	1000 rpm
Outer diameter	130 mm
Air gap thickness	0.3 mm
Number of rotor poles	8
Number of stator poles	6
Rotor pole angle	24°
Stator pole angle	22°
Stator windings	140 mm
Stator pole height	28 mm
Rotor pole height	11 mm

Fig. 2. 2-D FEA model of SRHM.

2.4. Estimation of torque and inductance profile of the 6/8 pole SRHM

In the SRHM the inductance of motor depends on position of the rotor. To find inductance profile of motor, rotor has to move from unaligned position to aligned position or vice versa. Initially, the rotor is kept at unaligned position. The excitation current of the motor is varied and the torque, flux linkage and inductance are calculated for that position. The procedure is repeated to determine the inductance, torque and flux linkage for all the rotor positions. The current vs. flux linkage profile determined using FEA is shown in Fig. 5. Fig. 6 shows the inductance profile of SRHM determined using FEA.
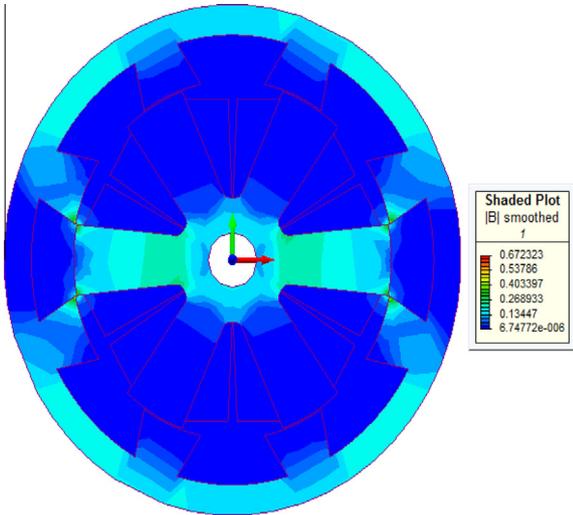

Fig. 1. Two dimensional view of SRHM.

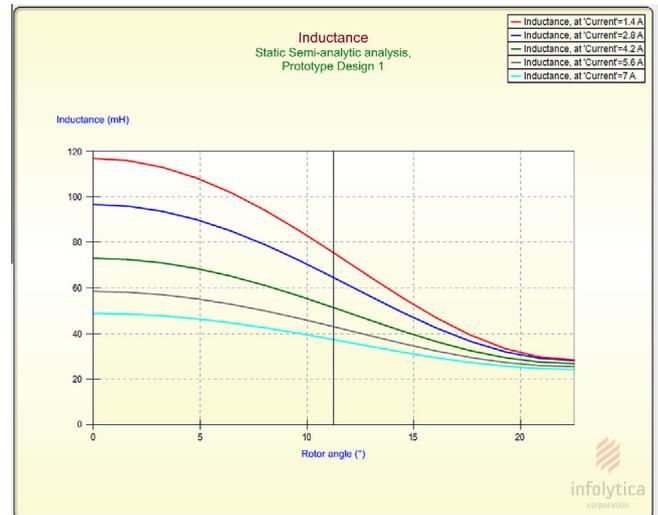**Fig. 3.** Flux density plot in the unaligned position.

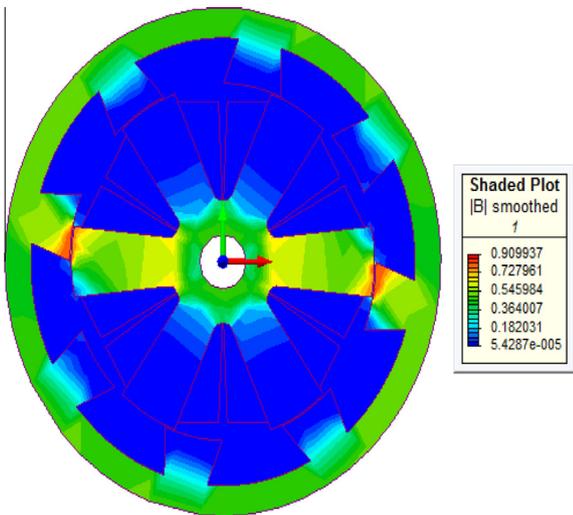**Fig. 6.** Inductance profile of 6/8 pole SRHM.

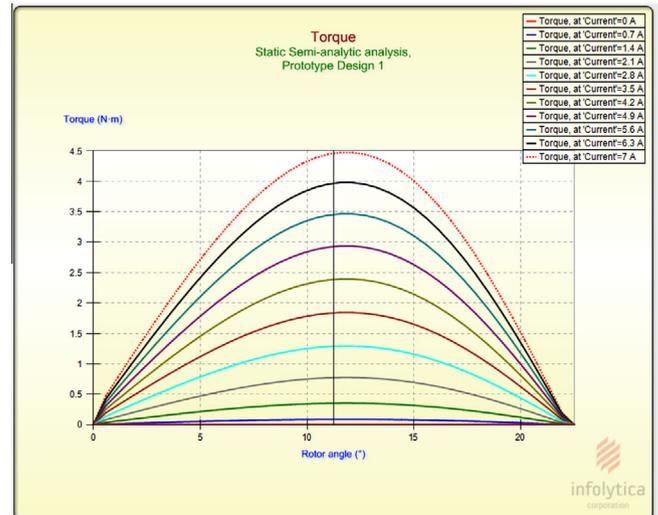
Fig. 4. Flux density plot in an intermediate position.
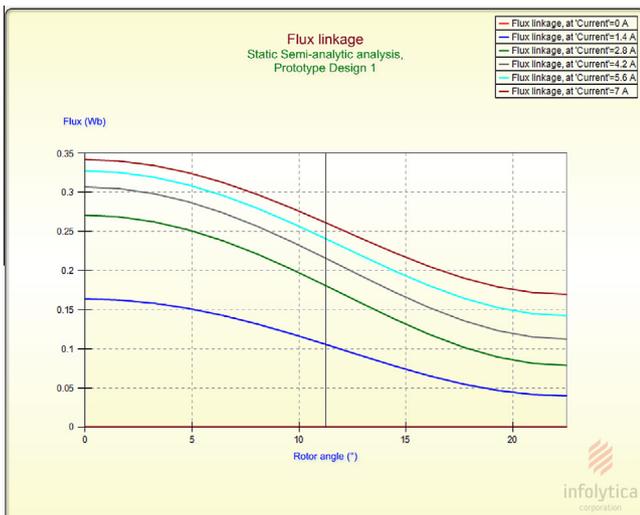

Fig. 7. Single phase torque profile at different currents.

Fig. 5. Current – flux linkage characteristics.

Table 3
Anticlockwise motion excitation sequence.

Rotor position	Excited phase
0–7.5	C
7.5–22.5	B
22.5–37.5	A
37.5–52.5	C

Table 4
Motion excitation sequence.

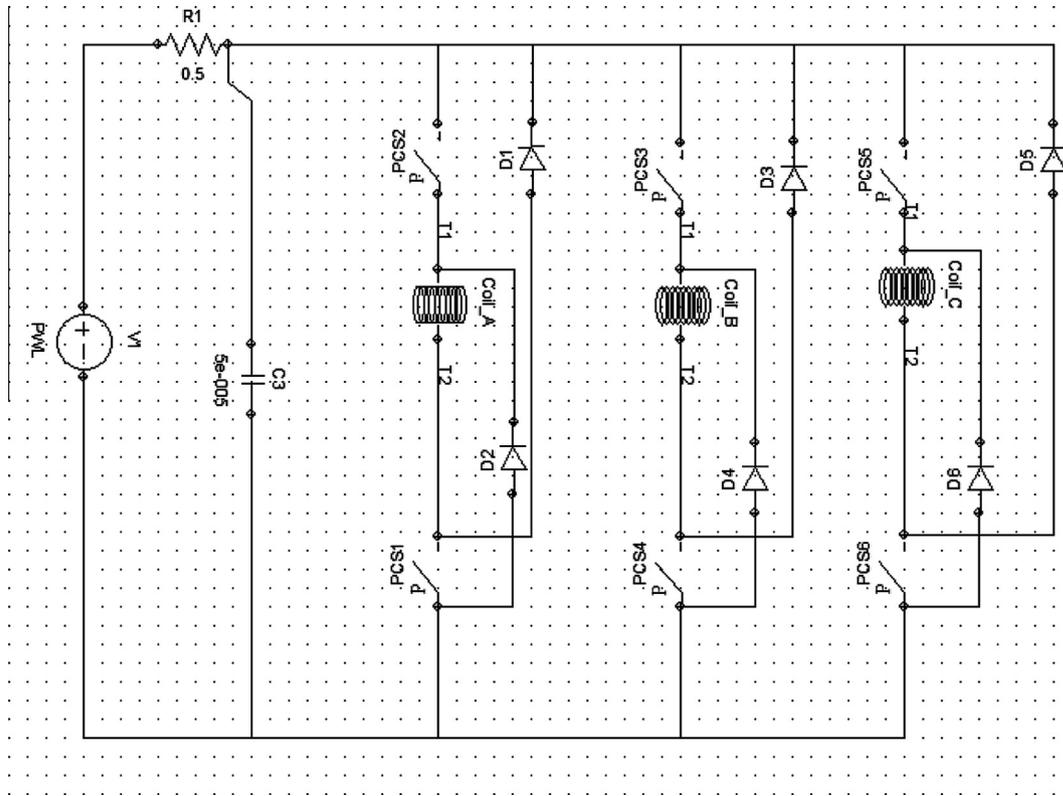| Rotor position	Excited phase
0–7.5	B
7.5–22.5	A
22.5–37.5	C
37.5–52.5	B

Fig. 8. Three phase model of the SRHM converter in circuit domain.
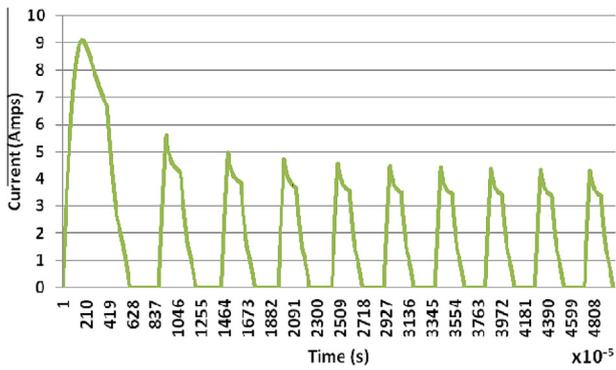

Fig. 9. Current waveform of phase A at 0.75 N m.

Fig. 11. Speed – torque characteristics.
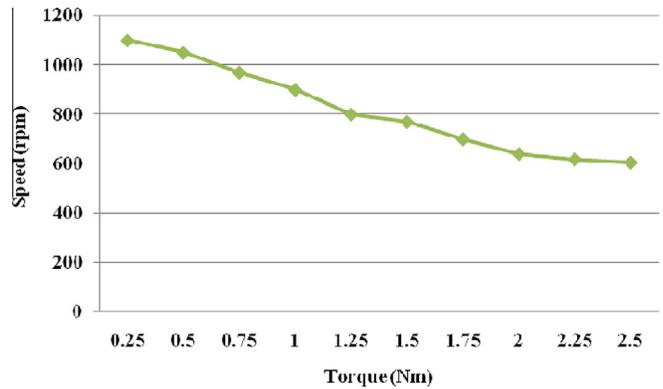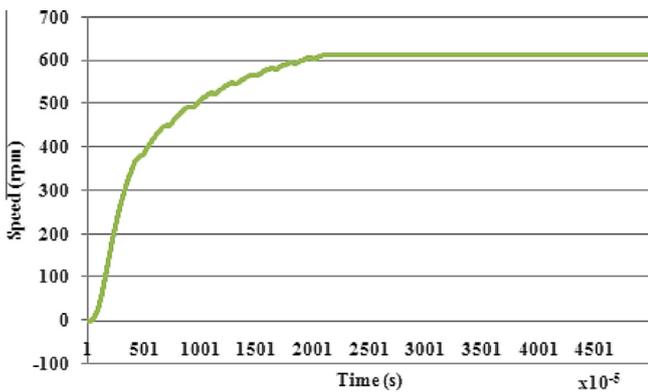

Fig. 10. Rotor speed at 36 V.

Fig. 12. Stator lamination and shaft with key.

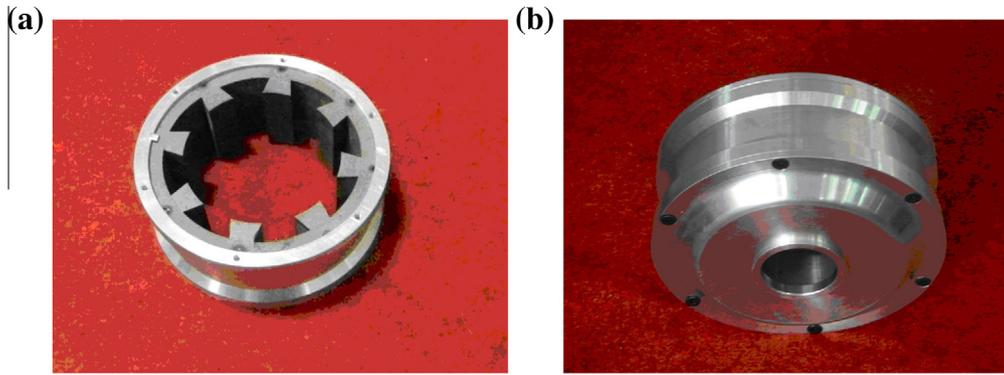**(a)**   **(b)**

Fig. 13. (a) Rotor Laminations with Rotor Sleeve (b) Rotor side brackets.
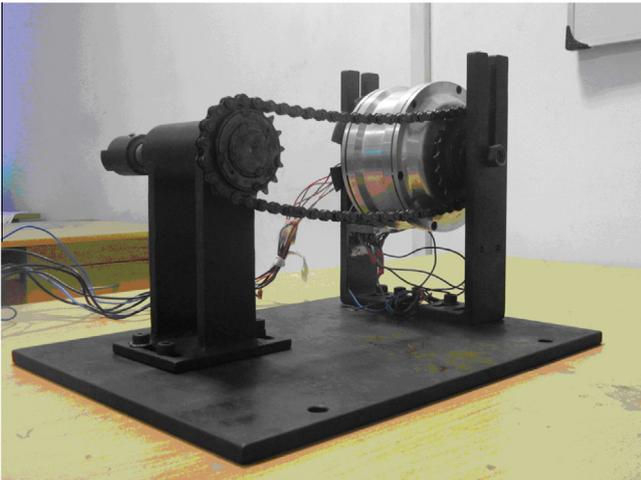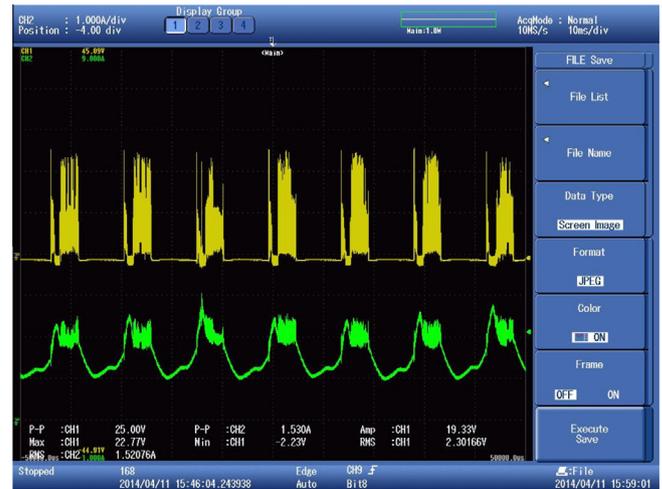

Fig. 14. Motor on test bench.

Fig. 16. Voltage and current waveforms.

Fig. 15. Experimental setup.

For a given current, the torque developed at the unaligned position is zero. When rotor moves towards the aligned position, the developed torque varies. Fig. 7 shows torque produced by the motor when one of the phases is excited at the rated current. It is found that the maximum value of torque is 4.4 N m and the average torque is 3.2 N m. Also the torque ripple calculated is 13.2%

2.5. Estimation of torque and speed profile using transient simulation

In SRHM phase windings, if current flows at the increasing inductance region, a motoring positive force is generated. The electromagnetic force is not affected by the polarity of the phase winding current and is dependent only on the translator position and the phase winding current magnitude. The sequences for backward and forward motions are shown in Table 3 and Table 4 respectively. Only one phase winding is energized during one third of stroke angle that is, 45^0. For single phase excitation, conduction period of phase A winding can be found to be between $7.5°$ and $22.5°$. Similarly, for clockwise movement of the rotor, the conduction period of phase A winding can be found to be between $37.5°$ and $50°$.

The complete circuit model is modeled in FEA software's circuit domain, and is shown in Fig. 8. PCS1, PCS2, PCS3, PCS4, PCS5 and PCS6 are the position controlled switches which connect and disconnect the phase windings to the supply according to the rotor position. Diodes D1, D2, D3, D4, D5 and D6 are fast acting devices during the freewheeling mode.

Fig. 9 shows current waveform of phase A when the stator windings are given a voltage of 36 V and rotor is given a load torque of 0.75 N m. Fig. 10 shows the time required for the rotor to reach steady state. It is shown that at a load torque of 2.5 N m, it reaches a speed of 611 rpm. Fig. 11 shows the speed – torque characteristics. As the load torque increases, the speed decreases.
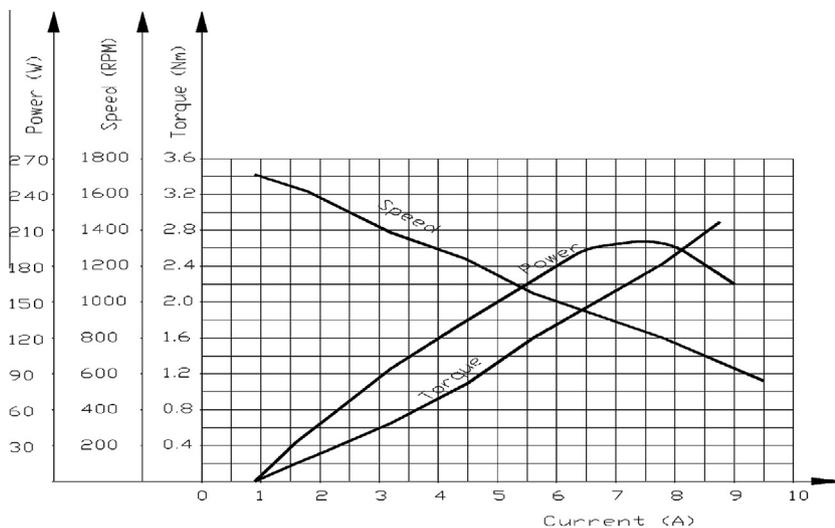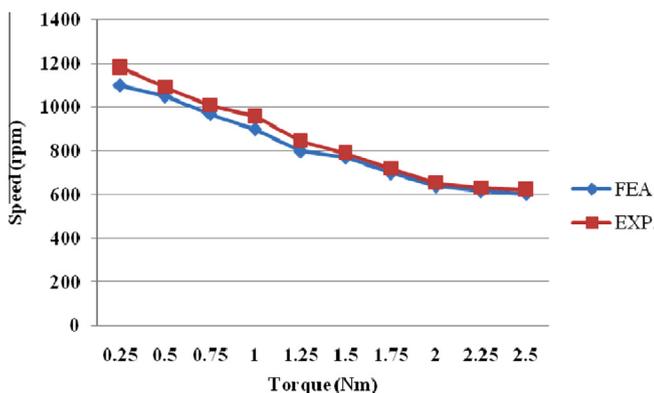
Fig. 17. Performance curves of SRHM.

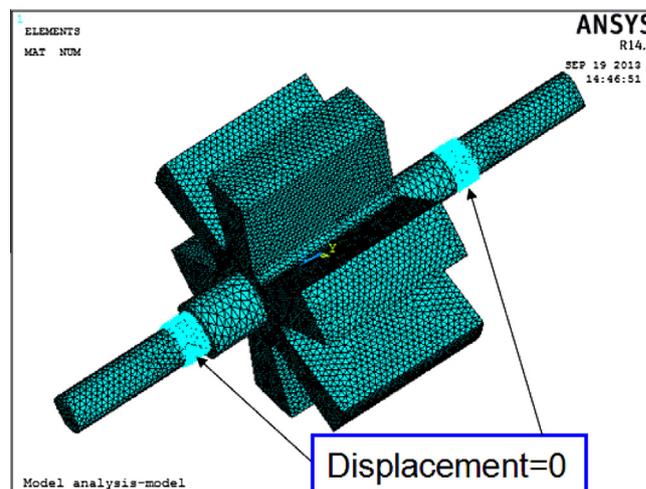**Fig. 18.** Comparison of FEA and test data.

Table 5
Natural frequencies of stator using analytical method.

Mode no.	Natural frequency (Hz)
1	838
2	2023
3	2459
4	3976
5	4018

Fig. 19. 3D model with boundary condition.

3. Fabrication and experimental verification

This section presents the fabrication and experimental verification of SRHM. The Hub motor structure consists of an internal stator fixed to the shaft of the motor. The rotor is on the external side and is attached to the rotating case. A rotating disc used for rotor position deduction is fixed to the rotating end case. Fig. 12 shows the stator lamination, shaft, key and bearings.

On both ends of the shaft, flatness is applied, so that the machine with the shaft can be seated on the test bench. Inner part of the machine houses the windings. End brackets cover the stator. Rotor has rotor laminations, sleeve, side brackets and a sprocket.

Fig. 13 (a) shows rotor lamination and rotor sleeve. Fig. 13 (b) shows the rotor sleeve connected to the brackets. Rotor lamination is welded at seven spots. A through hole is provided on the sleeve and the rotor laminations. A through piece holds the rotor laminations and the sleeve without slip.

In a hub motor, the stator is housed on the shaft and the load is applied on the rotor. Since the shaft cannot be loaded, the hub motor requires a test bench, specially designed for testing. Fig. 14 shows the test bench. Two vertical L-clamps are given grooves to house the shaft of the motor. On one of the L-clamp, an inverted L-clamp is placed for housing the rotor positions sensors. A sprocket is connected, on one end of the motor, to facilitate the connection of loading arrangement and on the other end of the motor a rotating disc is connected for sensing rotor position. The sprocket connected to the rotor is connected to the shaft of the clutch. Hub of the machine is fitted with a sprocket of a bicycle. The sprocket fitted to the motor is connected to a chain sprocket which is connected to a magnetic clutch. By changing the current flowing into the magnetic clutch, the torque applied on the motor is varied. A torque transducer is connected between the magnetic clutch and the chain sprocket to enable torque measurement. The photograph of the entire prototype setup is shown in Fig. 15.

Voltage and current are recorded for three phases using an oscilloscope and 'A' phase plot is depicted in Fig. 16. The speed – torque characteristics of the machine are given in Fig. 17. Fig. 18
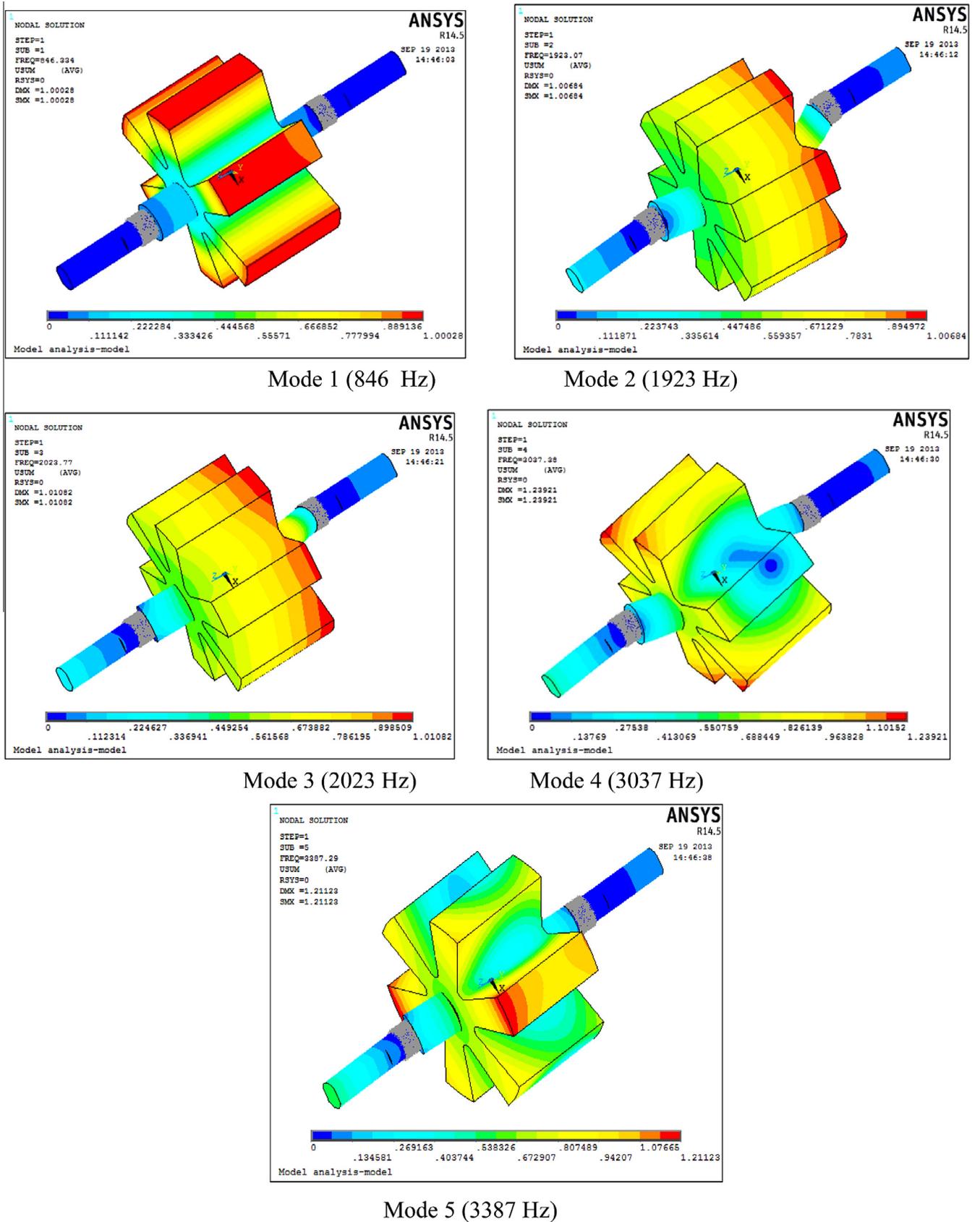
Mode 1 (846 Hz)

Mode 2 (1923 Hz)

Mode 3 (2023 Hz)

Mode 4 (3037 Hz)

Mode 5 (3387 Hz)

Fig. 20. Stator mode shape using 3-D analysis.

Table 6
Stator mode frequencies.

Mode no.	Stator mode frequencies (Hz)
1	746
2	1923
3	2023
4	3337
5	3387

shows the FEA and experiment results comparison of speed – Torque Characteristics of the machine. At no-load, the difference is 24% (app.). As the load torque increases, the difference is reducing. At rated torque of 2.5 N m, the difference between experiments and FE is 10% (app.). The maximum torque obtained during experiment is 2.95 N m at 8.6 A. Since the measured values are closely correlated with the predicted values there is no need for redesigning the machine parameters. Maximum power occurs at 7.5 A.
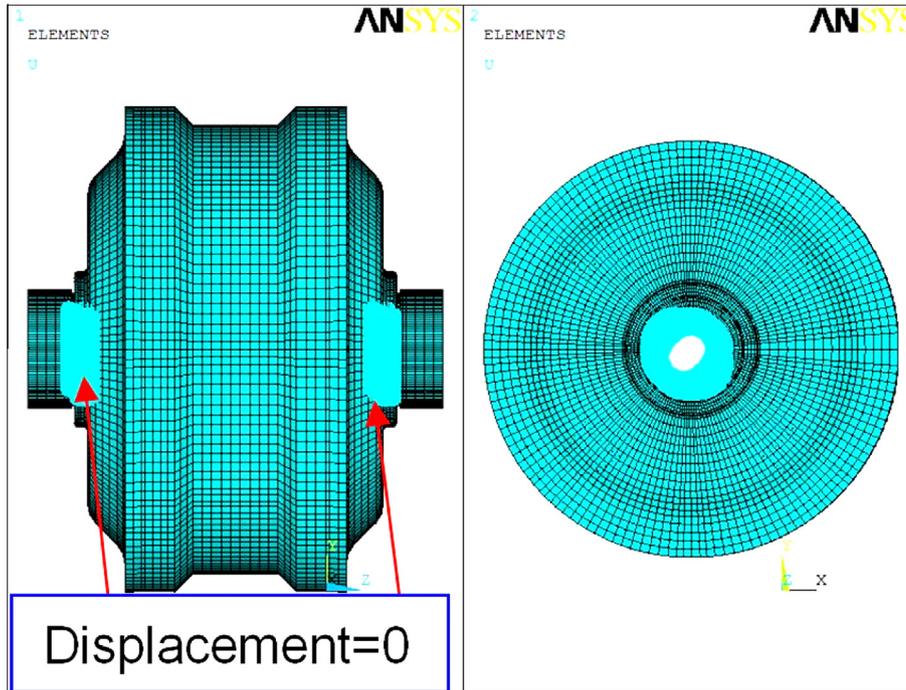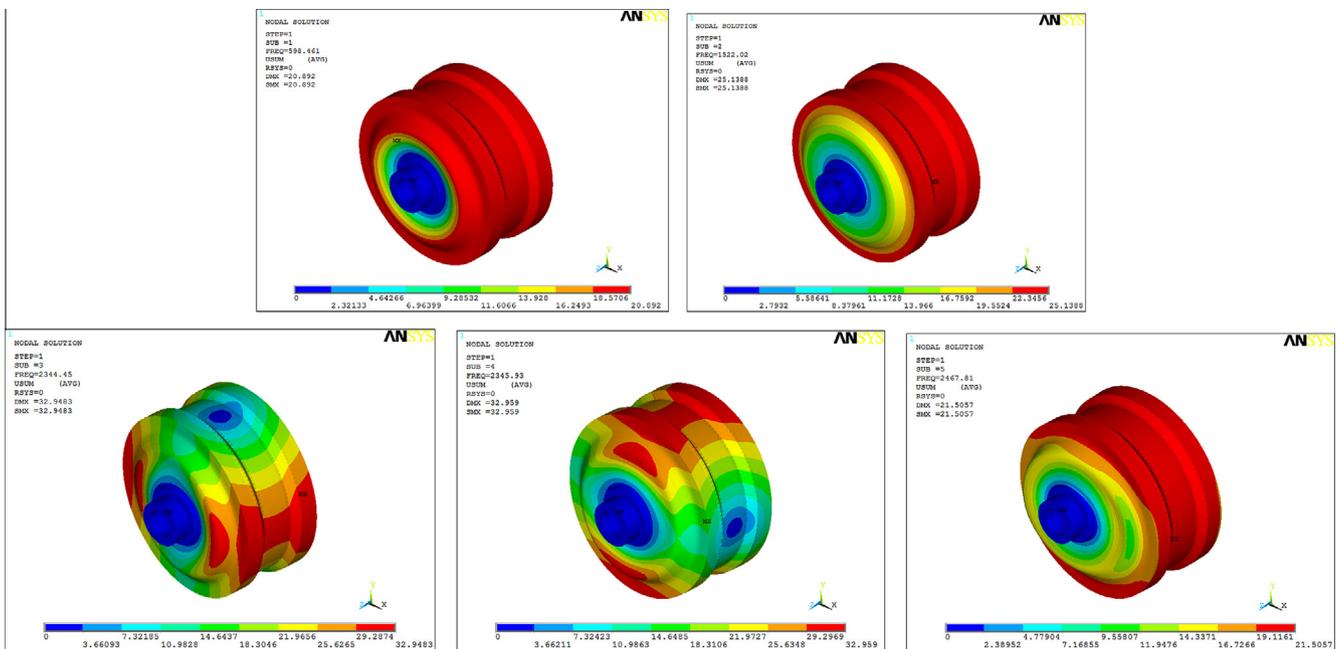

Fig. 21. Meshed model and boundary conditions.

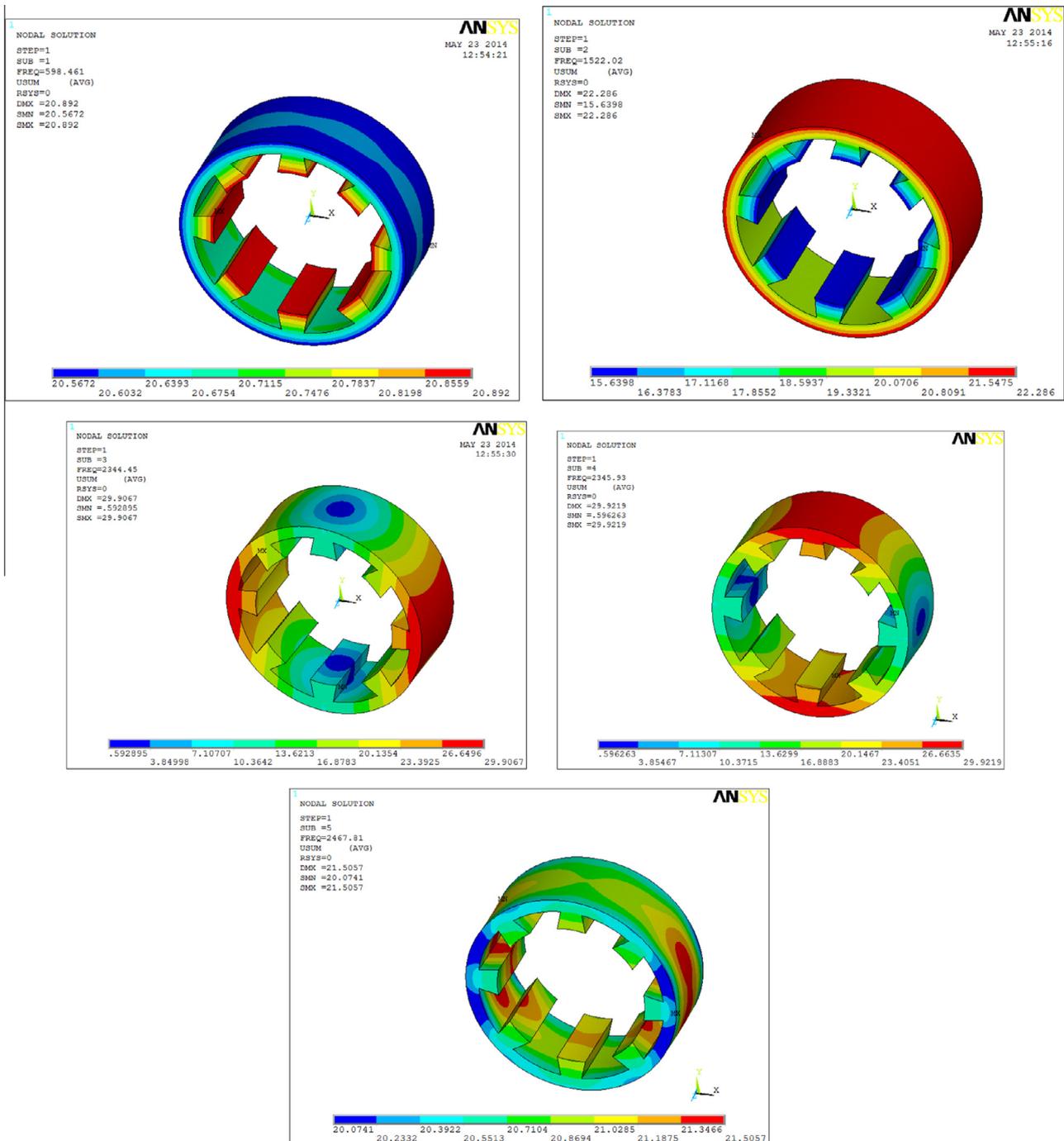**Fig. 22.** Rotor assembly mode shapes and modal frequencies.

Fig. 23. Rotor lamination mode shapes and modal frequencies.

4. Vibration and noise measurement

Vibration and noise are mainly due to the saliency on stator and rotor in SRHM. The vibration amplitude increases when the induced vibration frequencies coincide with the natural frequencies of SRHM. The vibrations create sound pollution and finally reduce the overall performance of the SRHM.

4.1. Estimation of resonant frequencies

The SRHM can operate at different speeds with a wide range of switching frequencies. The vibration and their magnitudes due to torque ripples and magnetic forces depend on the switching tech-

niques and frequencies. The vibration resonance will occur if the switching frequency coincides with the natural frequency of the SRHM. The natural frequency depends on the geometric design and can be calculated using mathematical methods [11]. The calculated first five mode frequencies are tabulated in the Table 5.

Unlike a conventional rotary motor, in the SRHM, the stator of motor is connected to the shaft which is fixed to the frame. Hence, the boundary conditions at the shaft are given zero. The meshed model with boundary condition is shown in the Fig. 19. The result of the analysis gives the first five mode frequencies and their displacement magnitudes of the model and it is shown in the Fig. 20. The stator mode frequencies are shown in Table 6.
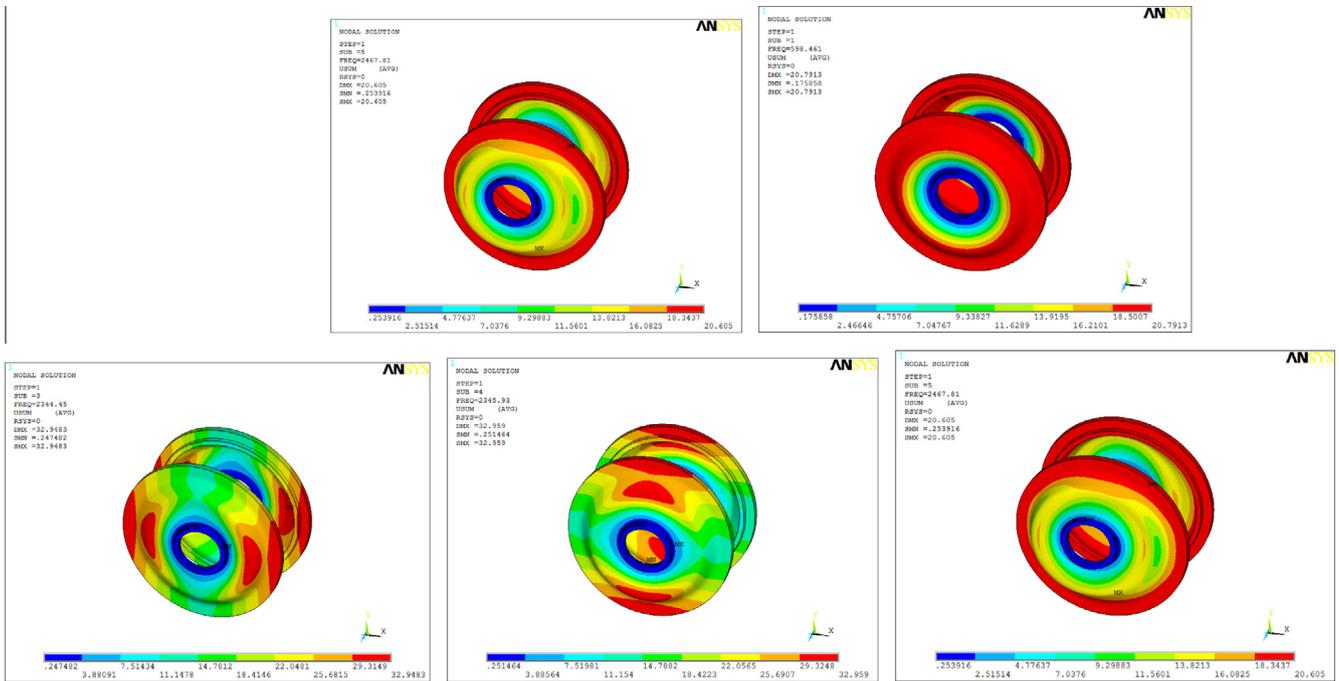
Fig. 24. Rotor casing mode shapes and modal frequencies.

Table 7
Rotor mode frequencies.

Mode no.	Rotor mode frequencies (Hz)
1	598.5
2	1522
3	2344
4	2345

4.2. Calculation of natural frequencies of rotor using 3D FEA

Inner surface of bearing is the one, which is not moving in the rotor assembly. Hence, the rotor is to be simulated as an assembly, not as a single component. A three dimensional model is created with SOLID45 element. Meshed modal and boundary conditions are shown in Fig. 21. Boundary condition such as displacement is given to the nodes. The modal analysis is performed to calculate model frequencies and the maximum mode frequency obtained is 2345 Hz. Rotor assembly mode shapes and model frequencies
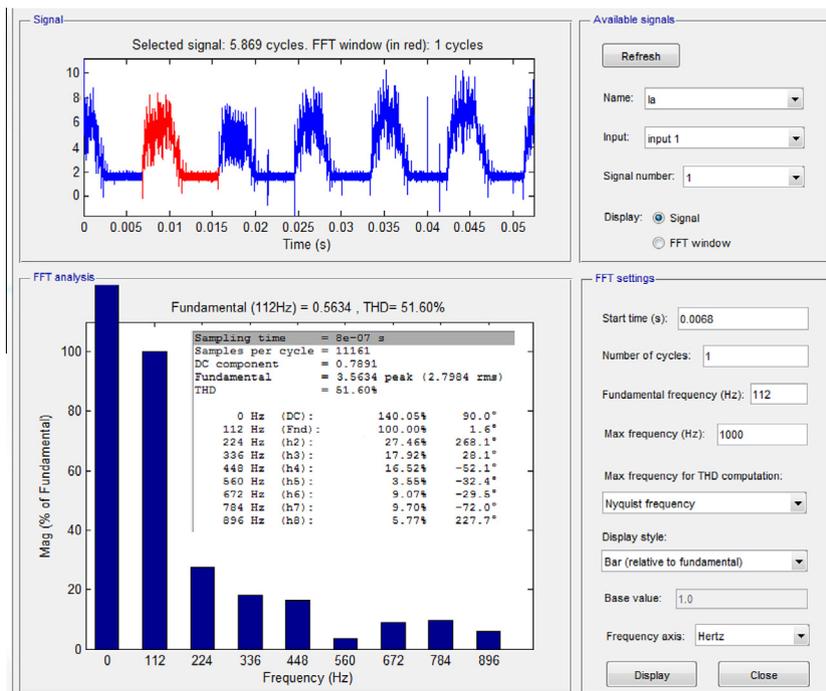

Fig. 25. Measured current waveform and harmonic component of waveform.

Table 8
Normal and tangential forces for different currents.

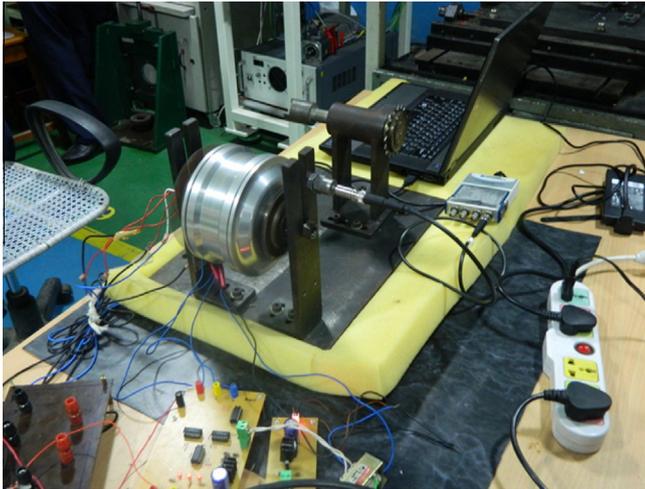| Order	Current (A)	Frequency (Hz)	Normal force (N)	Tangential force (N)
Fundamental	2.8	112	35	7
2nd	0.76888	224	5	0.5
3rd	0.50176	336	2	0.25
4th	0.46256	428	0.5	0.1

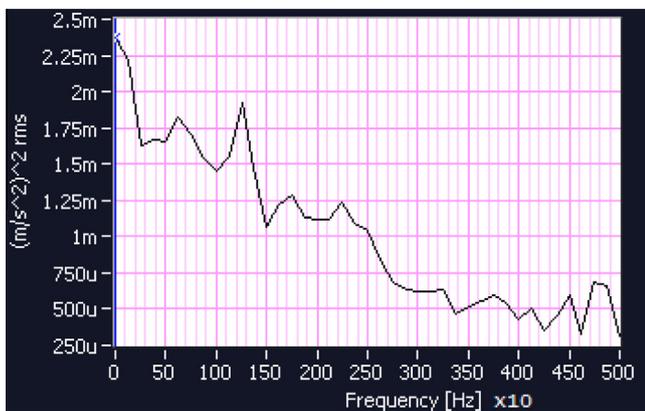**Fig. 26.** Experimental setup to measure vibration.

Fig. 27. Acceleration on measurement on SRHM.

are shown in Fig. 22. Rotor lamination mode shapes are shown in Fig. 23. The rotor casing mode shapes are shown in Fig. 24. The maximum frequency obtained is around 2467 Hz. Rotor assembly frequencies are enumerated in Table 7.

4.3. Estimation of vibration on stator using structural harmonic FEA

In the SRHM, the current is non-sinusoidal in shape and it contains harmonic components. These harmonic components generate forces on the stator in their respective frequencies. In this section, an investigation is made to study the structural deformation due to the non-sinusoidal current excitation. For the analysis, the SRHM is run under the condition specified above. Current waveform is measured using a current probe and a storage oscilloscope. The current

waveform is stored in csv format. Data of csv format is used in the FFT tool box of MATLAB SIMULINK to get the harmonic components. Fig. 25 shows the measured waveform and harmonic content of the current waveform. FFT analysis is made on the current waveform to separate the current components for their harmonic frequencies. For these currents the normal and tangential forces are calculated using the magnetic 2D FEA and is given in Table 8.

4.4. Experimental measurement of vibration

The vibration generated in the motor is measured using the accelerometer to validate the estimations. To measure the vibration an accelerometer is mounted on the hub of the motor. Fig. 26 shows the photograph of the experimental set up. Shear, ceramic type piezoelectric crystal, J352B is used. Displacement is a good measure at lower frequencies. In order to get displacement, the acceleration signal is integrated twice and to get velocity the signal is integrated once.

Using LABVIEW software, voltage measurement block is enabled and sample rate is fixed. Using this block, voltage signal is converted to acceleration. To get velocity and displacement, the acceleration signal is integrated once or twice respectively. Spectrum obtained from the experimental set up shown in Fig. 27.

It is observed from the experimental results that, the magnitudes of vibration are maximum at 700 Hz (nearer to first mode), 1250 Hz and at 2200 Hz (nearer to third mode) on the stator.

4.5. Noise measurement

The noises from electric machines are in the form of whine noise, i.e., tonal noise. (Typically in 400 Hz–2000 Hz range). The tonal nature of the whine noise from the electrical machines can be annoying to the passenger. Noise Measuring Device used here is made by Bruel-Kjaer and the type is 2250 Light. Fig. 28 shows the experimental setup for noise measurement. Measurement of noise using the A-weighted meter is taken at five different positions, at different speeds. The average of noise level of all the positions gives the noise level at that speed.

The noise spectrums for the speed of 250 rpm, 500 rpm, and 1000 rpm and at 1500 rpm are depicted in Figs. 29–32 respectively. Table 9 shows the comparison of noise levels at different positions of the machine

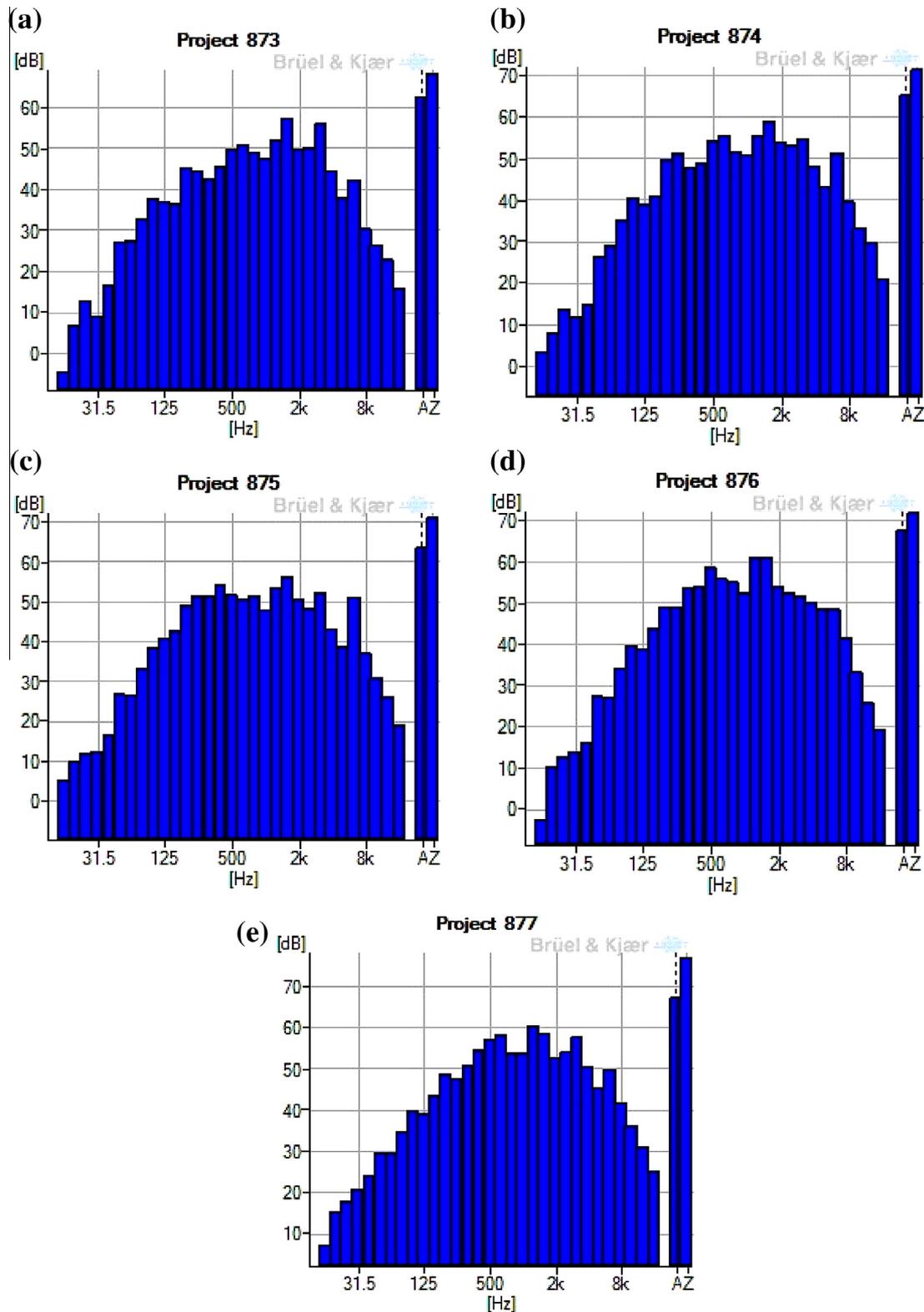**Fig. 28.** Experimental setup of noise measurement.

Fig. 29. Noise spectrum for the speed of 250 RPM at (a) shaft position (b) right side (c) left side (d) opposite to shaft position (e) top position.

From the Table 9, it is concluded that the noise level of the motor increases with increase in speed. This is due to the noise of the sprocket. The purpose of sprocket here is to connect the machine to the clutch. This sprocket will not have any influence in the working of the motor in EVs. Hence, the noise of sprocket need not be given an importance. Fig. 33 shows comparison of sound level at the five prescribed positions.
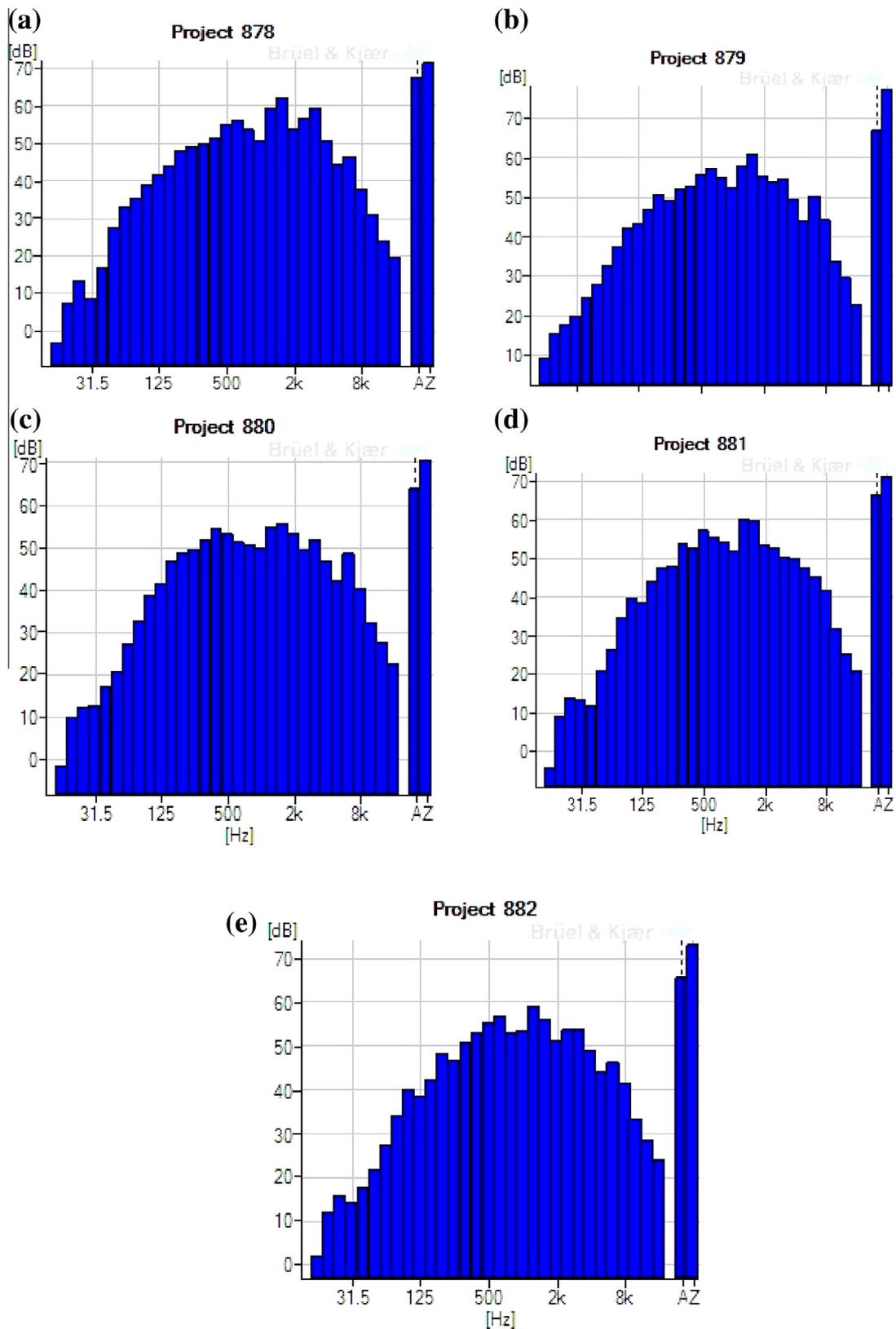
Fig. 30. Noise spectrum for the speed of 500 RPM at (a) shaft position (b) right side (c) left side (d) opposite to shaft position (e) top position.

5. Conclusion

A 262 W, 2.5 N m three phase 6/8 pole SRHM has been designed, analyzed, fabricated and tested. Detailed vibration anal-

ysis has been carried out on the SRHM to predict the magnitude of the ripple frequencies. The vibration on the prototype is measured using the accelerometer, coupled with a signal conditioner using LABVIEW. It is observed from the experimental results that, the
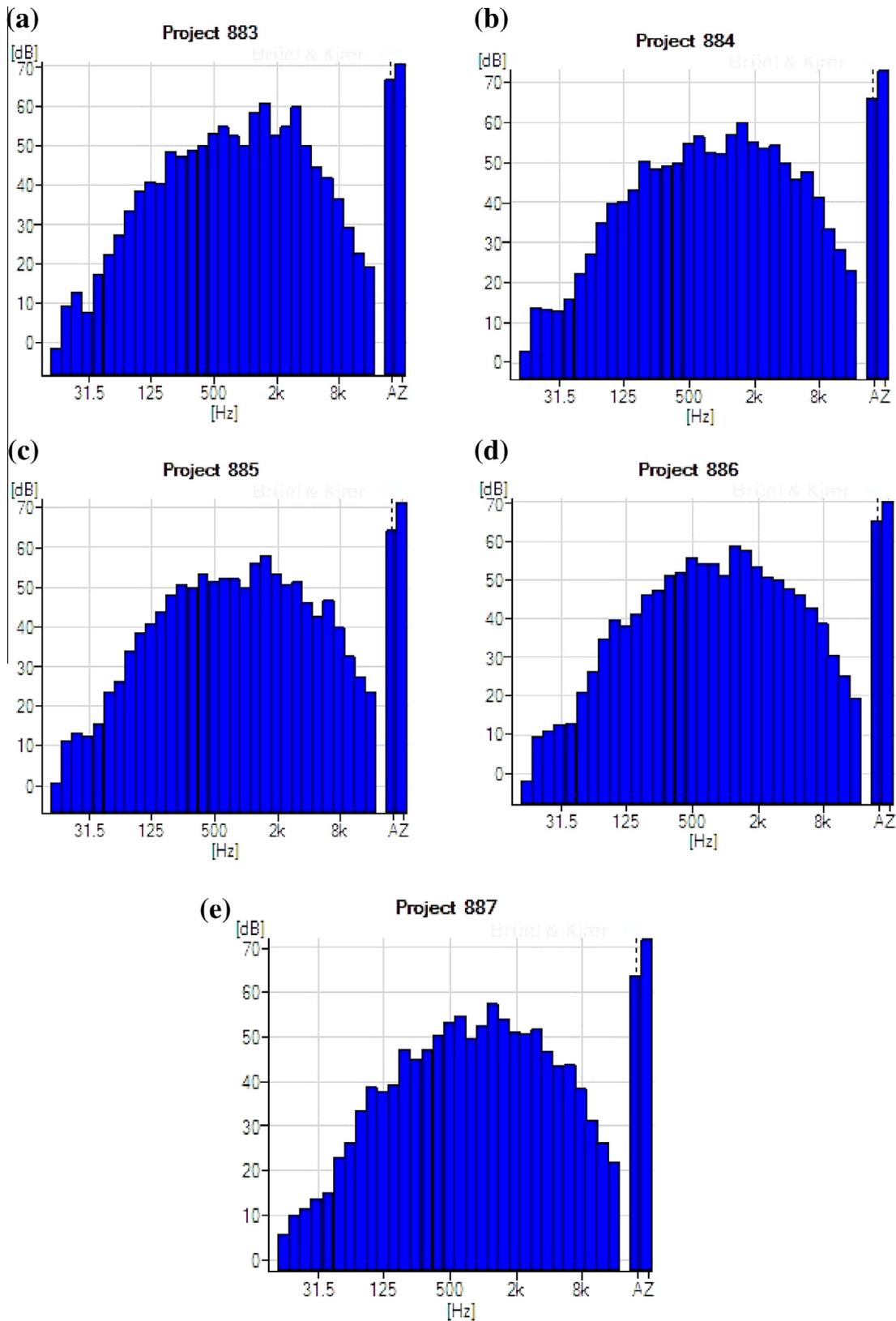
Fig. 31. Noise spectrum for the speed of 1000 RPM at (a) shaft position (b) right side (c) left side (d) opposite to shaft position (e) top position.

magnitudes of vibration are maximum at near the first and third modes on the stator. In order to measure noise accurately, the motor and the converter are placed in an anechoic chamber. Noise level of the machine is measured at different positions. Measurement has been made at different positions. Maximum noise level is 69.3 dB, near the hub of the machine.
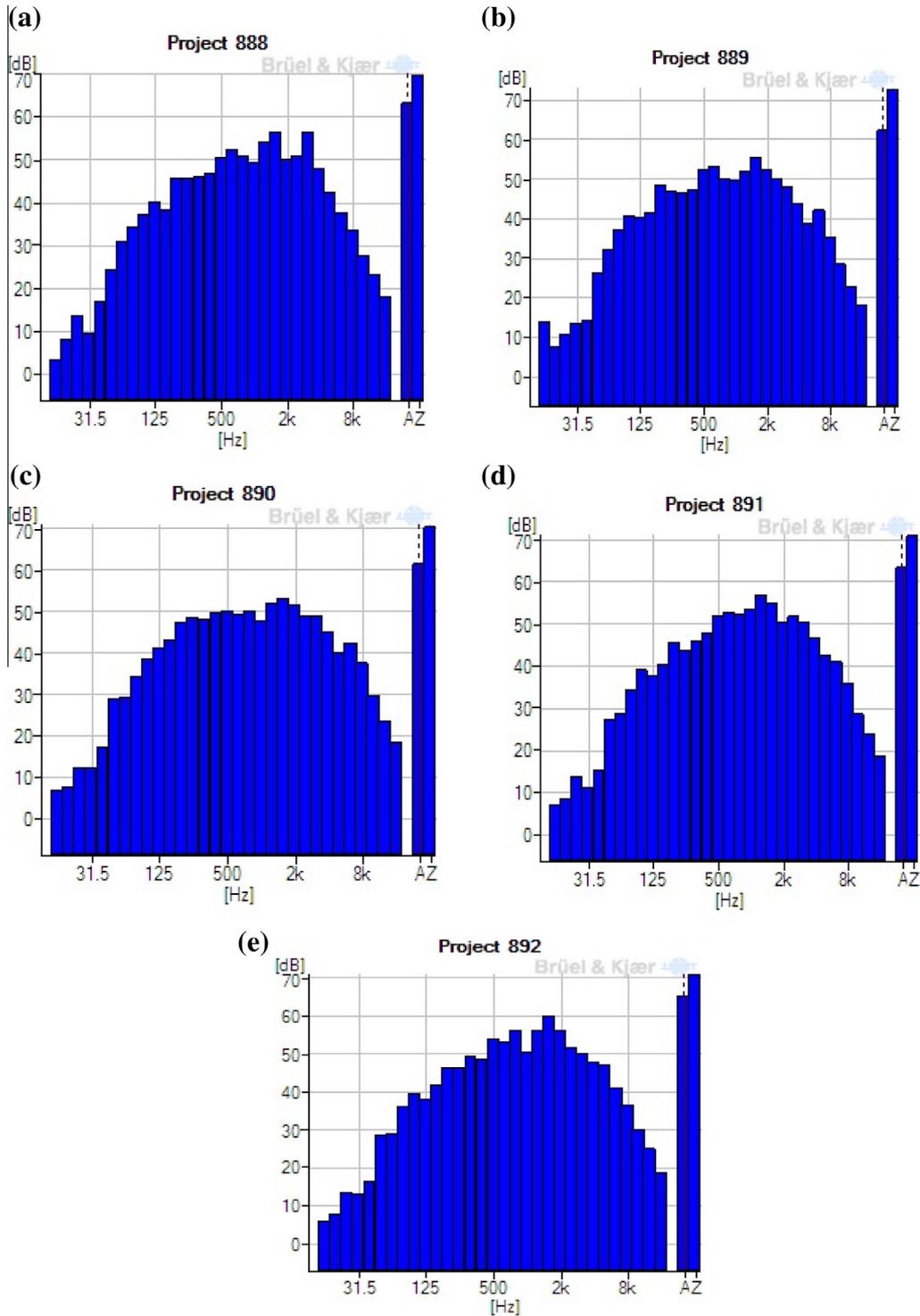
Fig. 32. Noise spectrum for the speed of 1000 RPM at (a) shaft position (b) right side (c) left side (d) opposite to shaft position (e) top position.

Table 9
Noise level for different speeds at different positions.

Position	Noise level at different speeds			
	500 rpm	750 rpm	1000 rpm	1500 rpm
Disc	62.6	63.3	64.3	67.6
Sprocket	65.4	65.9	66.8	69.3
Left	60.2	62.3	63.2	64
Right	61.3	62.4	64.1	65
Top	63.5	64.2	65.3	67.8
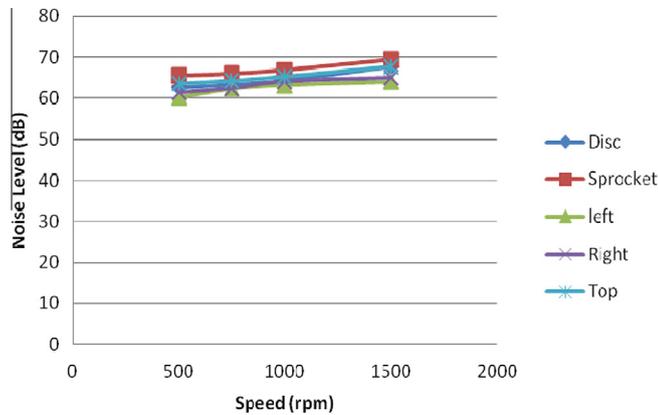
Fig. 33. Measurement of noise level in SRHM.

Acknowledgment

References

[1] T.S. Low et al., Design and analysis of 4-phase (in-hub) mini-switched reluctance motor for spindle motor in hard disc drive, in: Proc. ICPEDS, 1995, pp. 645–650.

[2] S.S. Ramamurthy, J.C. Balda, Sizing a switched reluctance motor for electric vehicles, IEEE Trans. Ind. Appl. 37 (5) (2001) 1256–1264.

[3] K. Cakir, A. Sabanovic, In-Wheel motor design for electric vehicles, in: Proc. 9th Int. Workshop AMC, 2006, pp. 613–618.

[4] P.C. Luk, P. Jinupun, An In-Wheel switched reluctance motor for electric vehicles, in: Proc. 5th IPEMC, vol. 3, CES/IEEE, 2006, pp. 1–5.

[5] Z. Qianfan, C. Shumei, T. Xinjia, Hybrid switched reluctance motor applied in electric vehicles, in: Proc. VPPC, IEEE, 2007, pp. 359–363.

[6] V. Petrus, Design and comparison of different switched reluctance machine topologies for electric vehicle propulsion, in: Proc. ICEM, XIX, 2010, pp. 1–6.

[7] X.D. Xue et al., Multi-objective optimization design of In-Wheel switched reluctance motors in electric vehicles, IEEE Trans. Ind. Electron. 57 (9) (2010) 2980–2987.

[8] C.J. Ifedi et al., Fault-tolerant In-Wheel motor topologies for high-performance electric vehicles, IEEE Trans. Indust. Appl. 49 (3) (2013) 1249–1257.

[9] R. Wrobel et al., Design considerations of a brushless open-slot radial-flux PM hub motor, IEEE Trans. Indust. Appl. 50 (3) (2014) 1757–1767.

[10] S. Prabhu et al., Vibration and thermal analysis of switched reluctance hub motor, Eur. J. Sci. Res. 68 (1) (Jan. 2012) 12–20.

[11] V. Chandrasekar, S. Prabhu, R. Arumugam, Design and implementation of a 250W, low speed switched reluctance hub motor, J. Electric. Eng. 12 (1) (2012) 167–174.

[12] S.P. Nikam, Sau Shambhu, B.G. Fernandes, Design of Switched Reluctance Motor based Electric Drive-train for Intra-Campus Two Wheeler, 39th Annual Conference of the IEEE Industrial Electronics Society, IECON, 2013, pp. 4612–4617. Nov. 2013.

[13] C. Ragupathi, V. Chandra Sekar, D. Susitra, Rotor Position Sensing and Converter for Switched Reluctance Hub Motor, International Conference on Computation of Power, Energy, Information and Communication, 2014, pp. 109–113. April.

[14] Jianing Lin, Nigel Schofield, Ali Emadi, External-rotor 6–10 switched reluctance motor for an electric bicycle, IEEE Trans. Transport. Electrification 1 (4) (2015) 348–356.